Video Article

Techniques for Processing Eyes Implanted With a Retinal Prosthesis for Localized Histopathological Analysis

David A. X. Nayagam[1,2,3], Ceara McGowan[1], Joel Villalobos[1], Richard A. Williams[2,3], Cesar Salinas-LaRosa[2,3], Penny McKelvie[2,3], Irene Lo[2,3], Meri Basa[2,3], Justin Tan[1], Chris E. Williams[1,3,4]

[1]Bionics Institute

[2]Department of Anatomical Pathology, St Vincent's Hospital Melbourne

[3]Department of Pathology, University of Melbourne

[4]Medical Bionics Department, University of Melbourne

Correspondence to: David A. X. Nayagam at DNAYAGAM@bionicsinstitute.org

URL: http://www.jove.com/video/50411
DOI: doi:10.3791/50411

Keywords: Medicine, Issue 78, Anatomy, Physiology, Biomedical Engineering, Bioengineering, Surgery, Ophthalmology, Pathology, Tissue Engineering, Prosthesis Implantation, Implantable Neurostimulators, Implants, Experimental, Histology, bionics, Retina, Prosthesis, Bionic Eye, Retinal, Implant, Suprachoroidal, Fixation, Localization, Safety, Preclinical, dissection, embedding, staining, tissue, surgical techniques, clinical techniques

Date Published: 8/2/2013

Citation: Nayagam, D.A.X., McGowan, C., Villalobos, J., Williams, R.A., Salinas-LaRosa, C., McKelvie, P., Lo, I., Basa, M., Tan, J., Williams, C.E. Techniques for Processing Eyes Implanted With a Retinal Prosthesis for Localized Histopathological Analysis. *J. Vis. Exp.* (78), e50411, doi:10.3791/50411 (2013).

Abstract

With the recent development of retinal prostheses, it is important to develop reliable techniques for assessing the safety of these devices in preclinical studies. However, the standard fixation, preparation, and automated histology procedures are not ideal. Here we describe new procedures for evaluating the health of the retina directly adjacent to an implant. Retinal prostheses feature electrode arrays in contact with eye tissue. Previous methods have not been able to spatially localize the ocular tissue adjacent to individual electrodes within the array. In addition, standard histological processing often results in gross artifactual detachment of the retinal layers when assessing implanted eyes. Consequently, it has been difficult to assess localized damage, if present, caused by implantation and stimulation of an implanted electrode array. Therefore, we developed a method for identifying and localizing the ocular tissue adjacent to implanted electrodes using a (color-coded) dye marking scheme, and we modified an eye fixation technique to minimize artifactual retinal detachment. This method also rendered the sclera translucent, enabling localization of individual electrodes and specific parts of an implant. Finally, we used a matched control to increase the power of the histopathological assessments. In summary, this method enables reliable and efficient discrimination and assessment of the retinal cytoarchitecture in an implanted eye.

Video Link

The video component of this article can be found at http://www.jove.com/video/50411/

Introduction

Retinal prostheses may soon become useful clinical interventions for treating various forms of severe vision loss. Certain conditions, such as retinitis pigmentosa (RP), result in the widespread degeneration of the photoreceptors in the eye; these are the cells responsible for transducing light into neural signals. However, some cells in other layers of the retina remain and are potential targets for electrical stimulation with a retinal prosthesis [1]. Early results from human clinical trials have been promising for electrode arrays implanted in the epiretinal [2,3], subretinal [4,5], and intrascleral [6] locations. These devices are made from different materials with different shapes, but they all use electrical pulses to activate the remaining viable neurons of the retina in order to create visual percepts.

Our wider group (Bionic Vision Australia) has developed a retinal implant that has progressed to a clinical pilot study with 3 RP patients implanted with suprachoroidal electrode arrays (Clinical Trial Number: NCT01603576). **Figure 1A** shows this suprachoroidal prototype retinal prosthesis.

Patient safety is paramount in clinical studies and thus, before commencing human trials, we performed extensive acute and chronic testing in preclinical models (**Figure 1B**). Histopathological assessments were essential to refine the surgical procedures, iterate through electrode design, and ultimately establish the safety of the implant. To maintain an efficient workflow dovetailed with standard clinical pathology practices, a paraffin embedding technique was employed. It was also desirable to utilize staining procedures comparable with clinical standards, such as haematoxylin and eosin (H&E), which are readily interpreted by pathologists. We also wanted a technique that could be adapted for immunohistochemical analyses, in order to facilitate further cellular evaluation of the tissues.

The biocompatibility of the implant materials, and the safety of chronic electrical stimulation, need to be carefully assessed. It is important to be able to examine the histopathology of the ocular tissue adjacent to the individual stimulating electrodes within the array. However, the arrays needed to be removed prior to processing the samples so they can be tested, and because their metallic components could not be readily sectioned. Consequently, our established tissue preparation did not permit localization and mapping of tissue with respect to the implanted electrodes [7]. In addition to the lack of a tissue localization method, the standard formaldehyde-based fixation and processing techniques resulted in widespread artifacts and detachment of the retinal due to the differential shrinkage of the various layers of the eye (**Figure 2**). Due to the non-homogeneity of the retina, it was difficult to make valid comparisons with control tissue, particularly for quantitative measurements. These combined limitations complicated accurate assessments of the potential damage caused by our implanted arrays.

Here we present novel techniques for overcoming these limitations. We have modified specialized eye fixation and processing techniques [8-10] to maintain compatibility with paraffin-based histology. We have modified standard histological and immunohistochemical stains to give comparable results, based on feedback from clinical pathologists. After rendering the scleral tissue translucent, a dye-based color-code was employed to mark the ocular tissue adjacent to each individual electrode, before removing the array from the suprachoroidal space. By marking the electrode array and the individual electrode sites, samples could be accurately collected from electrode adjacent regions. Matched samples could be gathered from the control eye in order to facilitate pairwise comparisons.

Protocol

1. Enucleation and Post-Fixation

This protocol assumes that the subject has been implanted unilaterally with a suprachoroidal electrode array.

1. Prepare postfix solutions in glass Schott bottles.
    a. Davidson's fixative solution, 2x 100 ml
        - 2 ml formalin (37% formaldehyde)
        - 10 ml glacial acetic acid (99.7%)
        - 35 ml ethanol (98%)
        - 53 ml distilled water

    b. 50% ethanol, 2x 100 ml
    c. 70% ethanol, 2x 100 ml
2. Transcardially perfuse subject with warm (37 °C) heparinized saline followed by cold (4 °C) neutral buffered formalin (10%).
3. Tie sutures at the superior limbus (or a location that is remote from the suprachoroidal array) of both eyes - in line with a rectus muscle, to serve as a landmark.
4. Enucleate eyes, maintaining any external leads from the implanted eye.
5. Place each eye in 100 ml of Davidson's fixative solution and leave to post-fix at room temperature.
6. After 18 - 36 hr in Davidson's fixative, transfer to 50% ethanol (room temperature) for 6 - 8 hr, then finally to 70% ethanol (room temperature).
7. Refrigerate samples at 4 °C and store until dissection.

Intact and pressurized eye globes have been stored in this manner for up to 3 months without adversely affecting the resultant histology.

2. Identification and Tissue Mapping

The above fixation protocol (step 1) has rendered the sclera translucent and the array is now visible - including the individual electrode sites (**Figure 3**).

1. Remove the implanted globe from ethanol and carefully trim away excess tissue, including conjunctiva and Tenon's capsule. Trim optic nerve to a 2 - 3 mm length (**Figure 3A**).
2. Using a histological dye marking scheme, label the electrodes with a predefined color code, taking care not to smudge the dye.

- We chose a commercially available suite of specialized histological dye (refer to appendix). Small amounts of the dye were carefully applied with a fine tipped paint brush (Roymac size 00) to the tissue and allowed to air dry for up to 5 min.
- For our purposes, we have chosen: green for the active electrode(s) that was(were) stimulated maximally, at suprathreshold levels, for the duration of the study; red for other active electrodes; yellow for the larger diameter return electrodes; and blue for additional guides and/or anatomical distance markings (**Figures 3B and 3C**).
- Some trial and error may be required to find a dye that is stable throughout the subsequent steps. For example, in **Figure 4**, it can be seen that the green dye was more resilient than the red dye. Diluting the dye in 70% ethanol helps improve lipid penetration and tissue coating.
- It is useful to sketch or photograph the dyed globe for future reference.

3. Return to 70% ethanol to dehydrate the dye.
4. Repeat step 2.1 for the unimplanted control globe.
5. Using the sutures from step 1.3, align the control eye and the implanted eye as a mirrored pair.
6. Place a silicone template (with the same dimensions as the electrode array) in the mirrored location on the control eye as the implant is located on implanted eye (*N.B.* the translucent sclera and the dye markings from step 2.2 allow ready visualization of the implanted array position).
7. Perform steps 2.2 and 2.3 for the control eye, so that each implanted electrode site has a control pair in an anatomically comparable (*i.e.* mirror matched equivalent) location.

3. Dissection and Embedding

1. Remove the implant array from the eye and remove the front of the eye (including the cornea, iris and lens). Remove the vitreous fluid from the remaining eye cup (posterior chamber).
2. Dissect the implanted eye into multiple representative strips (~2 mm thickness) each containing a subset of the dye marked regions (**Figure 3D**). Note that the orientation of the strips should be selected to assist in assessing various aspects of the tissue response to the implant[7].

It is useful, for future reference, to make a record of which dye regions are present on each strip and their relative locations (and colors).

3. Place the strip on its side into a shallow pool of liquefied agar (4%; 80 - 90 °C) with the side to be cut first facing downwards (**Figure 3E**).
4. Once the agar has set, cut around the sample and place into a tissue cassette supported by foam inserts (**Figure 3F**).
5. Repeat steps 3.1-3.3 for the control eye - taking care to dissect mirror-matched strips.
6. Process all cassettes *via* standard (automated overnight) paraffin processing technique.
7. Embed processed tissue in paraffin with the side to be cut first facing downwards.

4. Cutting and Staining

1. Cut paraffin blocks into 5 µm sections referring regularly to the notes from Steps 2 and 3.
2. Collect sections from each of the dyed regions and mount on slides.

The region immediately adjacent to each dyed spot of sclera can now be assessed with confidence that it was in closest proximity to the corresponding electrode in the array (**Figure 4**).

3. Stain or perform immunofluorescence as desired. Example stains and immunohistochemistry shown in **Figure 5** are: H&E; Luxol fast blue (LFB); cresyl violet; Masson's trichrome blue; periodic acid schiff (PAS); Perls' Prussian blue stain; anti-glutamine synthetase (GS); anti-neurofilament protein (NF); anti-glial fibrillary acidic protein (GFAP) and 4',6-diamidino-2-phenylindole (DAPI).
4. Standard and special stains were performed as detailed:
    1. H&E staining was performed according to the protocol provided by Leica multistainer bath array ST5020 (Leica Biosystems).
    2. LFB and cresyl violet (modified from [11]):
        1. Dewax in 3 changes of xylene (3x 2 min) and 2 changes of ethanol (100%, 100%) (2x 1 min) and rinse in tap water (45 sec).
        2. Hydrate sections to 95% ethanol.
        3. Place in LFB solution [11] at 37 - 42 °C (overnight).
        4. Rinse off excess stain with 70% ethanol.
        5. Rinse in distilled water.
        6. Place in dilute lithium carbonate (8%) (few seconds).
        7. Differentiate in 70% ethanol (few seconds).
        8. Rinse in distilled water.
        9. Repeat steps 4.4.2.6 to 4.4.2.8, if necessary, until background is colorless.
        10. Place in cresyl violet acetate working solution at 37 °C (10 min).
        11. Do not wash in water.
        12. Dehydrate in 3 changes of absolute alcohol (1x 30 sec, 2x 20 sec) and 3 changes of xylene (1x 1 min 30 sec, 2x 1 min).
        13. Mount and coverslip with DPX.
    3. Masson's trichrome blue (modified from [11]):
        1. Dewax as per 4.4.2.1.
        2. Bring sections to water (2 min).
        3. Stain the nuclei using Weigert's iron haematoxylin (2 min).
        4. Wash in tap water, rinse in distilled water.
        5. Stain in Biebrich scarlet-acid fuchsin solution (5 min).
        6. Rinse in distilled water.
        7. Differentiate in phosphomolybdic-phosphotungstic acid until collagen is pale pink (6 min).
        8. Rinse in distilled water.
        9. Counterstain in aniline blue (1 min).
        10. Wash well in 1% acetic acid (1 min).
        11. Dehydrate, mount and coverslip as per 4.4.2.12 and 4.4.2.13.
    4. PAS (modified from [11]):
        1. Dewax as per 4.4.2.1.
        2. Oxidize in 1% periodic acid (15 min).
        3. Wash in running water then distilled water.
        4. Stain in Schiff's reagent (15 min).
        5. Wash in water (5 min).
        6. Counterstain with Harris haematoxylin (1 min).
        7. Wash briefly in tap water.
        8. Differentiate in 0.5% acid alcohol (1 dip).
        9. Wash well in tap water.
        10. Blue in Scott's tap water (1 min).
        11. Wash well in water.

12. Dehydrate, mount and coverslip as per 4.4.2.12 and 4.4.2.13.

5. Perls' Prussian blue stain as described in [11].

5. Immunofluorescence staining was performed as detailed:
   1. Dewax as per 4.4.2.1.
   2. Rinse in distilled water (2x 5 min).
   3. Perform antigen retrieval using 0.01% citrate buffer, pH 6 at 75 - 80 °C (20 min) and allow to cool in 0.01% citrate buffer solution (20 min).
   4. Wash sections in phosphate buffered saline (PBS) (2x 5 min).
   5. Permeabilize the cell membrane in wash buffer solution (10 min).
   6. Incubate in serum block solution (2 hr).
   7. Incubate sections in a single primary antibody diluted in antibody diluent (10% normal goat serum/0.1% Triton X-100/PBS) (overnight in fridge). The titre of each primary antibody used is shown in Table 1.
   8. After overnight incubation, wash sections in wash buffer solution (5x 3 min). From this point on, keep sections in the dark.
   9. Incubate sections in the corresponding secondary antibody at a titre of 1:500 for a specific duration (see **Table 1** for details).
   10. Wash sections in wash buffer solution (3x 5 min).
   11. Incubate sections in DAPI (1:25,000 / PBS) (30 min).
   12. Wash sections in wash buffer solution (3x 5 min).
   13. Mount and coverslip using fluorescent mounting media.

Test samples and control samples are ready for pairwise comparison.

Representative Results

Figure 4 shows a representative section obtained from cutting the sample depicted in **Figure 3**. The section was cut at 5 µm thickness and stained with H&E according to the protocols described above. The gross shape of the sample strip is preserved with minimal differential tissue artifacts (**Figure 4A**). Both dye markings were visible on the sclera, although the green dye was more resilient than the red (**Figure 4B**). The retinal layers were not artifactually detached and the retinal morphology is preserved (**Figure 4C**). The retinal tissue adjacent to the dye markings, which corresponds to the location of the electrodes in the array, can be readily identified.

Figure 5 shows representative special staining and immunohistochemistry of tissue sections prepared according to the current protocol. Refer to **Figure 5** caption and Supplementary Materials for more detail on the specific stains and the modifications made to their usage. Post-modification, these stains and immunohistochemistry were equivalent to established standards - as verified by pathologists.

Type of primary antibody and titre (in parenthesis)	GFAP (1:1500)	NF200 (1:100)	GS (1:100)
Type of secondary antibody and titre (in parenthesis)	Alexa Fluor 594	Alexa Fluor 488	Alexa Fluor 488
Duration of incubation of secondary antibody	1 hr	2 hr	45 min

Table 1. Antibody Type, Titre and Duration of Labeling.

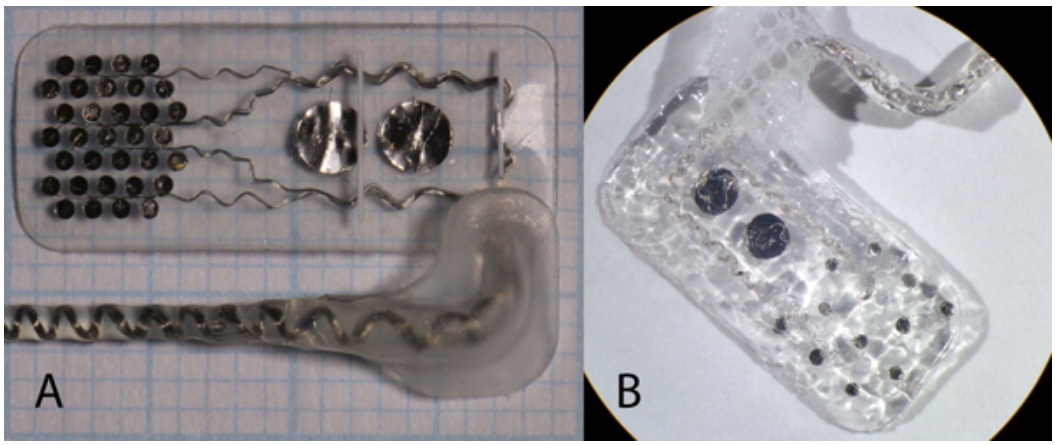

Figure 1. Suprachoroidal Prototype Electrode Array. A) Macro photograph of a clinical grade molded array. **B)** Photomicrograph of a handmade preclinical array.

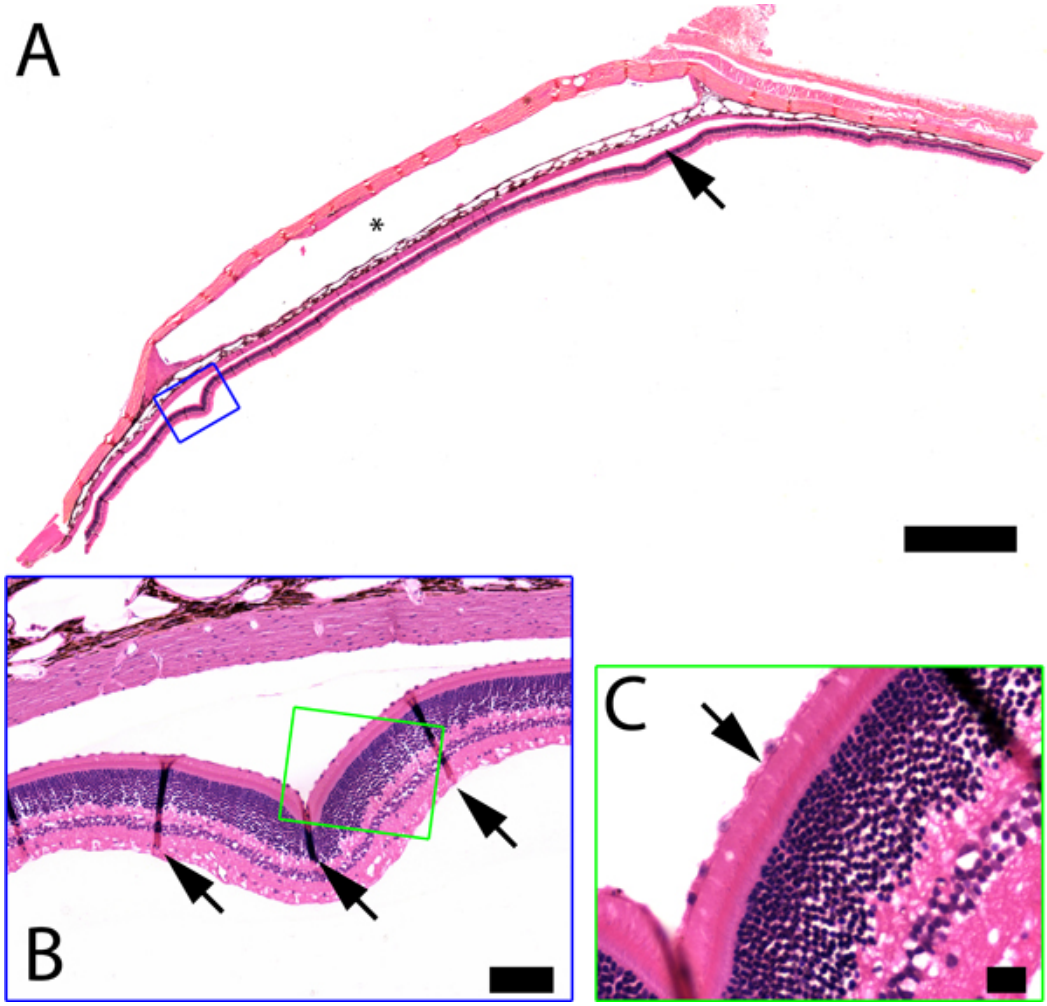

Figure 2. Former Retinal Histology. Standard histological methods were used to prepare these, H&E stained, sections of an eye implanted with a suprachoroidal electrode array. **A)** An orthogonal section through the electrode array cavity (depicted by a star). The retina is detached from the outer eye tissue. This is particularly evident beneath the implanted region (arrow). It is impossible to determine which portion of retina was adjacent to each individual electrode of the array. Scalebar = 1 mm. **B)** A higher magnification of the boxed region in Panel **A**. There are several, regularly spaced, artifacts in the retinal layers (arrows), as well as major detachment from the tapetal layer (the reflective layer in feline eyes). Scalebar = 100 µm. **C)** A higher magnification of the boxed region in panel **B**. Arrow indicated the outer segments of the photoreceptors, as well as the pigmental epithelium, which remain intact, suggesting that the detachment was an artifactual side-effect of the processing, as opposed to being caused by an *in vivo* trauma or pathology. Scalebar = 20 µm.

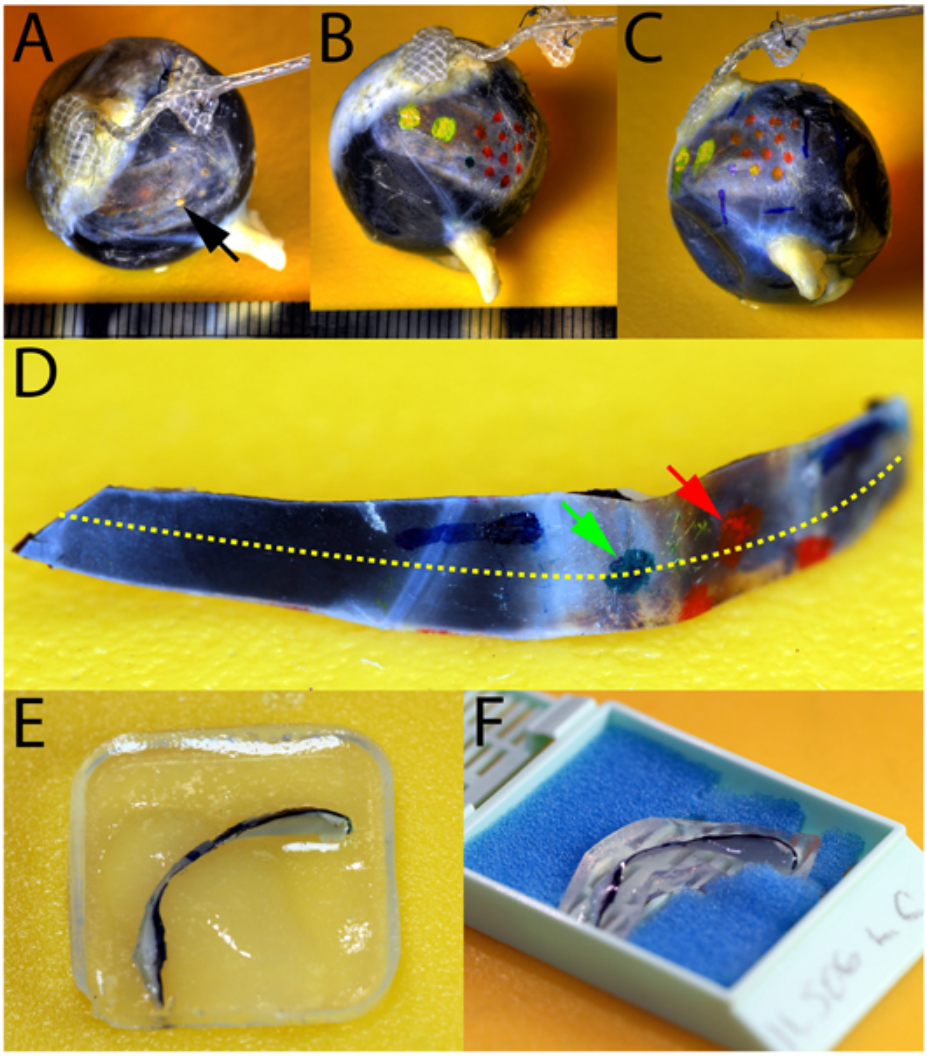

Figure 3. Localization and Dissection of Electrode-Adjacent Tissue. A-D) High dynamic range macro photographs of an enucleated eye, with a suprachoroidal electrode array *in situ.* **A)** Post fixed with Davidson's fixative, and prior to array removal, the translucent sclera enables visualization of the individual electrodes in the array (single example indicated with arrow). **B)** The electrodes are marked with a predefined dye color. **C)** Dye markings at regular spacing from anatomical landmarks are used to maintain consistency across experiments. **D)** Upon removal of the array, the eye is dissected by hand into sample strips. Colored arrows indicate two of the electrode adjacent sites on the sclera. Yellow dashed line indicates plane of sectioning. **E)** Macro-photograph of sample strip embedded within an agar block. **F)** Macro photograph of the agar-embed sample strip from Panel **E**, cut out and placed in an embedding cassette supported by foam biopsy pads to minimize movement of the section during processing.

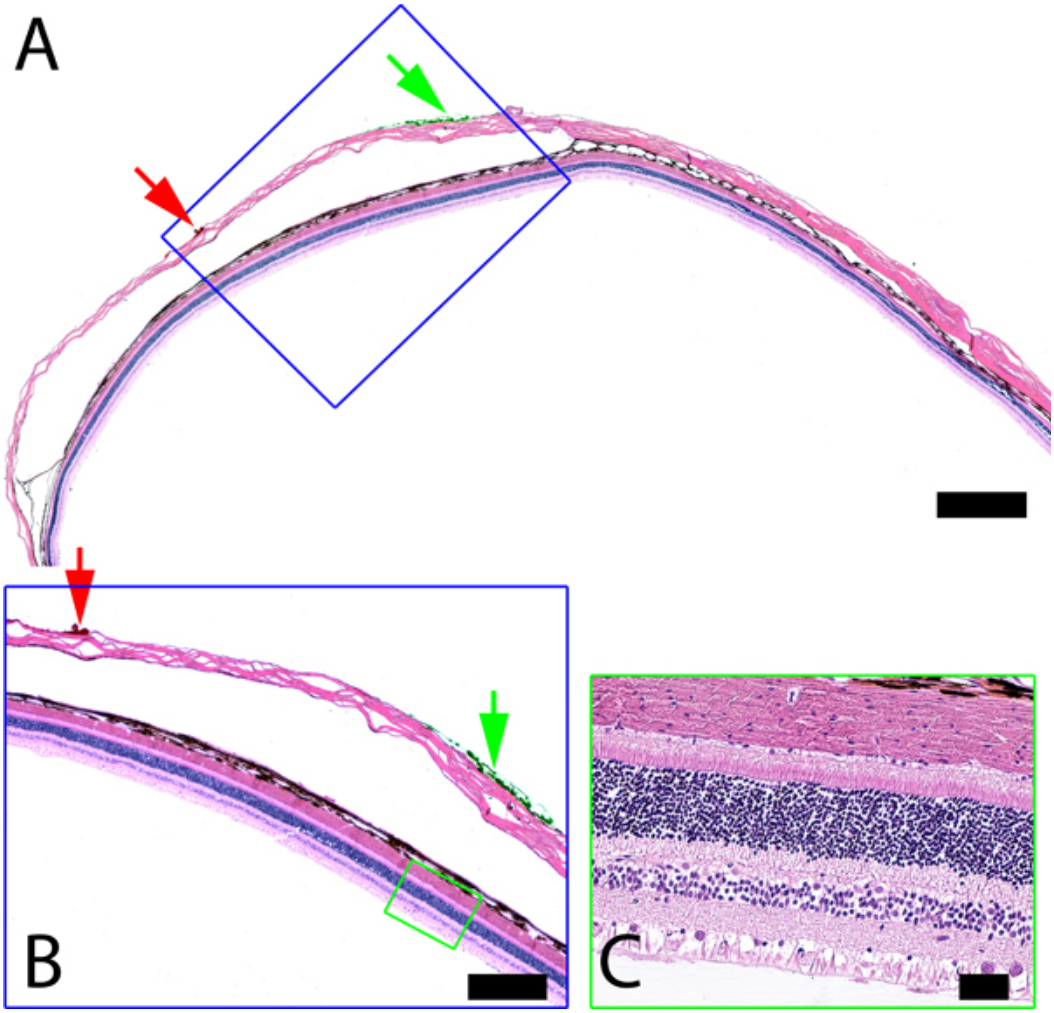

Figure 4. New Retinal Histology. The above sample strip (from **Figure 3D**), containing the electrode pocket, was paraffin embedded, sectioned at 5 µm and stained with H&E. **A)** Green and red dyed regions (indicated by arrows, same as **Figure 3D**) are visible in a section taken at the level of the yellow dashed line in **Figure 3D**. Scale bar = 1,000 µm. The retina is not detached, neither beneath the array pocket nor remotely. **B)** The boxed region from Panel **A** with visible red and green dye indicated by arrows, and intact retina throughout. Scale bar = 500 µm. **C)** The boxed region from Panel **B**, showing the intact, attached, retina adjacent to the green dye. Scale bar = 50 µm. Knowing that the location of the dye indicates the position of an electrode, we can confidently assess the adjacent retinal tissue for damage, if any, caused by electrical stimulation.

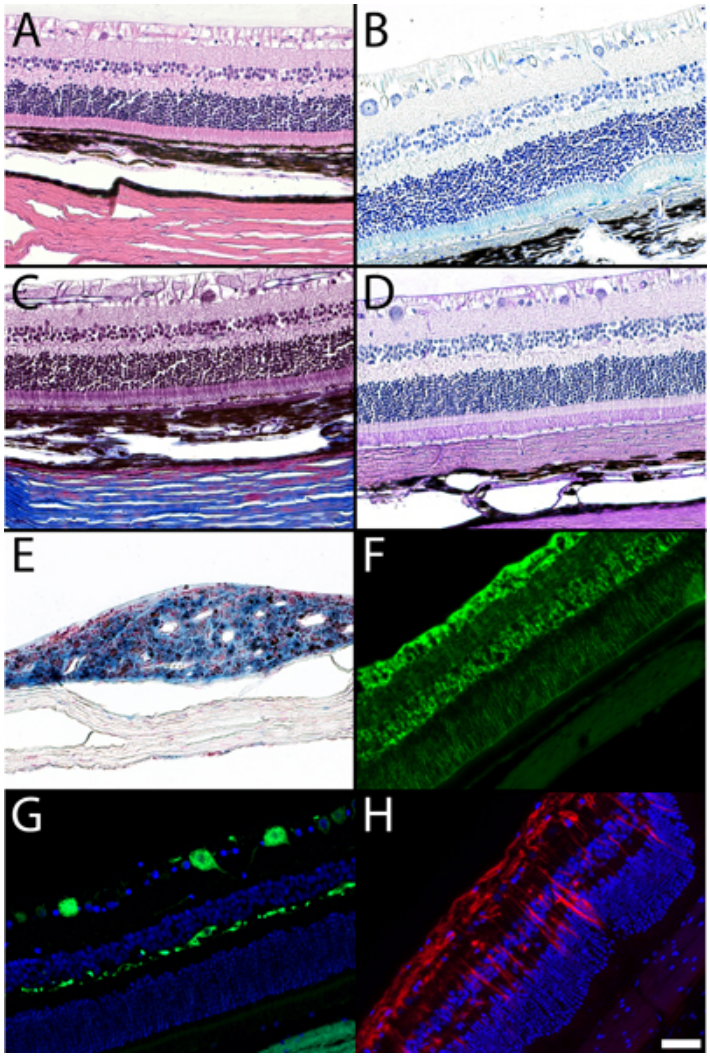

Figure 5. Examples of modified retinal cytohistochemistry using special stains and immunofluorescence. The use of Davidson's fixative, as opposed to standard formalin fixation techniques, required alterations to the usual staining protocols, as outlined in the main protocol text. Pathologists have confirmed that these modifications resulted in equivalent staining. **A)** H&E; haematoxylin stains cell nuclei purple while eosin stains cell cytoplasm, collagen and supportive tissue various shades of pink. **B)** LFB stains myelin blue while the cresyl violet counterstain can be used to identify ganglion cells by staining Nissl bodies within the perikaryon blue and highlighting the satellite cells surrounding the cells. **C)** Masson's trichrome blue; the Biebrich scarlet-acid fuchsin solution stains muscle fibers red, while the aniline blue stains the collagen, in this case sclera, blue. **D)** PAS; glycoprotein components of basement membrane and connective tissue components are stained purple, while the haematoxylin counterstains cell nuclei purple. **E)** Perls' Prussian blue; at the site of haemorrhage, the formation of haemosiderin from degraded red blood cells and release of iron complexes produces a purple color while the addition of neutral red stain colors lysosomes red. **F)** GS; this neurotransmitter degrading enzyme found in Müller cells [13] (green), can be seen extending in both directions with the Müller cell bodies in the inner nuclear layer and Müller cell endfeet forming the inner limiting membrane. **G)** NF-200; this heavy chain cytoskeletal protein (green) found in the cell soma and processes, crosslinks with other neurofilaments to maintain the structure of neurons [14,15]. Ganglion cells and their axons can be seen in the ganglion cell layer and nerve fiber layer, while axons of horizontal cells located at the outer boarder of the inner nuclear layer in the feline retina, are also highlighted. Counterstaining with DAPI (blue) allows visualization of retinal layers. **H)** GFAP; this cytoskeletal protein (red) proliferated in Müller cells and astrocytes during gliosis [16], can be seen lining the nerve fiber layer with Müller cells forming thin extensions through the inner to outer retinal layers. Counterstaining with DAPI (blue) allows for visualization of the retinal layers. Scale bar = 50 µm in all panels. The inner retina is shown at the top of each image; the outer retina is shown at the bottom of each image, excluding Panel **E**, which shows subscleral reaction.

Discussion

Assessing the safety of the implant is a primary consideration for preclinical studies. Before a retinal prosthesis can be implanted in humans it is essential to verify that it will not cause any harm. This requires an assessment of both the implant biocompatibility [17-23] as well as any potential damage that could be caused by chronic electrical stimulation [24-26]. Experience with similar neural prostheses, such as the cochlear implant, provides insight into the broad range of stimulation, and physical, parameters that do not cause tissue damage [27]. However, the retina has different characteristics to other implantation sites and therefore precise safety limits (such as maximum charge density) cannot be assumed from previous studies in other systems. Charge densities are highest at the active electrode sites and this corresponds with the greatest

potential for damage. Therefore a method for localizing the tissue directly adjacent to the individual active electrodes would greatly increase the usefulness of these studies. The tissue adjacent to specific regions of the implant may also be highlighted for closer inspection. This targeted approach permits fewer sections to be analyzed, whilst retaining confidence that the "worst case scenario" was examined.

The scleral dye localization method described here has been extensively tested with hand-shaped and molded silicone/Pt electrode arrays [28-30]. It has been used with thin-film polyamide arrays [7,31] and also thin-film silicone/Pt arrays [32]. Some retinal prosthesis studies employed "bullet shaped" electrodes with intrascleral implantations [33]. The present technique should be effective for assessing this type of electrode arrays. Feline eyes with thin sclera (thickness at posterior pole 90 - 200 µm) allowed visualization of individual electrodes in an array. However, even if individual electrodes were not visible, their positions could be readily inferred using a silicone template when the outline of the array can be seen (similar to that used in step 2.6).

The dye mapping limits the need to obtain non-relevant tissue sections as only sections with the dye present are obtained. The ability to accurately infer electrode position not only allows relevant histopathological analysis and greater statistical power, but has a major impact on time and cost management by reducing the quantity of slides and blades used as well as the cost of labor. The use of dye that is adherent and can withstand tissue processing whilst also being visible in unstained tissue sections is an important initial consideration. Knowledge of the location of the dye and orientation of the tissue at dissection and during embedding assists the cutting process. This includes correctly orientating the block to achieve a section that is not obliquely cut and gives a full representation of the tissue. It is therefore important that the person performing the cutting is present at the time of dye application, dissection and embedding.

The overall protocol is robust to minor alteration, particularly with fixation timings. However, the eye dissection and dye marking steps are delicate procedures that benefit from good manual dexterity to avoid damaging the specimen. Whilst Davidson's fixative has proved effective for reducing artifactual detachment of the retina near an implant, it does not prevent direct mechanical damage during dissection. Davidson's fixative was not readily compatible with some special histological and immunohistochemical procedures. Therefore there was a need to modify/optimize these steps as detailed above. Incremental changes in staining times and concentrations were made until the optimum result was achieved - for more details, refer to the supplementary materials.

Quantification of retinal histology remains problematic. The retina is non-homogeneous and both the thickness and the cell density change with increasing distance from area centralis [34,35]. Therefore, neighboring tissue within the implanted eye cannot be used for comparisons and a control eye is employed instead. Pairwise matching of each section with the control eye gives us a more powerful statistical comparison of pathological changes; efficacy and safety outcomes with retinal prosthetics are better assessed when comparing the fellow eyes in a subject [36]. Special care must be taken to minimize oblique cutting as this would affect quantification.

In summary, the methods described above have significantly improved our histopathological analysis, which in turn has led to a more efficient preclinical workflow. The results of preclinical studies using these methods directly led to a clinical trial in which 3 RP patients have been safely implanted with suprachoroidal retinal prostheses. These methods are relevant both to retinal stimulators and other ocular implants where the pathological response to long term implantation needs to be evaluated. This method provided worthwhile advantages for maintaining the cytoarchitecture and registration of the pathology to regions of interest on the implant. Although not specifically tested, a modification of these procedures may be used in other species and other anatomical locations, particularly where an array is implanted superficially.

Disclosures

Authors have nothing to disclose.

Acknowledgements

The authors wish to thank: Ms. Alexia Saunders and Ms. Michelle McPhedran for experimental assistance; Ms. Helen Feng for electrode fabrication; Dr. Penny Allen and Dr. Jonathan Yeoh for surgical assistance; Staff of the Royal Victorian Eye and Ear Hospital's Biological Research Centre for animal care; Prof. Rob Shepherd for general guidance throughout; and Dr. Bryony Nayagam and Mr. Ronald Leung for critical comments on a draft form of the manuscript.

This work was performed at the Bionics Institute and St Vincent's Hospital, Melbourne. Funding was provided by the Ian Potter Foundation, the John T Reid Charitable Trusts, and the Australian Research Council through its Special Research Initiative in Bionic Vision Science and Technology grant to Bionic Vision Australia (BVA). The Bionics Institute acknowledges the support it receives from the Victorian Government through its Operational Infrastructure Support Program.

References

1. Santos, A., Humayun, M.S., *et al.* Preservation of the inner retina in retinitis pigmentosa. *Arch. Ophthalmol.* **115**, 511-515 (1997).
2. Humayun, M.S., Weiland, J.D., *et al.* Visual perception in a blind subject with a chronic microelectronic retinal prosthesis. *Vision Res.* **43**, 2573-2581 (2003).
3. Roessler, G., Laube, T., *et al.* Angiographic findings folowing tack fixation of a wireless epiretinal retina implant device in blind RP patients. *Graefes. Arch. Clin. Exp. Ophthalmol.* **249**, 1281-1286 (2011).
4. Chow, A.Y., Chow, V.Y., *et al.* The artificial silicon retina microchip for the treatment of vision loss from retinitis pigmentosa. *Arch. Ophthalmol.* **122**, 460-469 (2004).
5. Zrenner, E., Bartz-Schmidt, K.U., *et al.* Subretinal electronic chips allow blind patients to read letters and combine them to words. *Proc. R. Soc. B.* **278**, 1489-1497 (2011).
6. Fujikado, T., Kamei, M., *et al.* Testing of semichronically implanted retinal prosthesis by suprachoroidal-transretinal stimulation in patients with retinitis pigmentosa. *Invest. Ophthalmol. Vis. Sci.* **52**, 4726-4733 (2011).

7. Villalobos, J., Allen, P.J., *et al.* Development of a surgical approach for a wide-view suprachoroidal retinal prosthesis: evaluation of implantation trauma. *Graefes. Arch. Clin. Exp. Ophthalmol.* **250**, 399-407, doi:10.1007/s00417-011-1794-6 (2012).
8. Latendresse, J.R., Warbittion, A.R., Jonassen, H., & Creasy, D.M. Fixation of testes and eyes using a modified Davidson's fluid: comparison with Bouin's fluid and conventional Davidson's fluid. *Toxicol. Pathol.* **30**, 524-533 (2002).
9. Agrawal, R.N., He, S., *et al. In vivo* models of proliferative vitreoretinopathy. *Nat. Protoc.* **2**, 67-77 (2007).
10. Margo, C.E. & Lee, A. Fixation of whole eyes: the role of fixative osmolarity in the production of tissue artifact. *Graefes. Arch. Clin. Exp. Ophthalmol.* **233**, 366-370 (1995).
11. Bancroft, J.D. & Gamble, M. *Theory and practice of histological techniques*., 6 edn., Churchill Livingstone, (2008).
12. Horobin, R.W. & Bancroft, J.D. *Troubleshooting histology stains*., Churchill Livingstone, (1998).
13. Pow, D.V. & Robinson, S.R. Glutamante in some retinal neurons is derived solely from glia. *Neuroscience.* **60**, 355-366 (1994).
14. Lewis, S.E. & Nixon, R.A. Multiple phosphorylated variants of the high molecular mass subunit of neurofilaments in axons of retinal cell neurons: characterization and evidence for their differential association with stationary and moving neurofilaments. *J. Cell Biol.* **107**, 2689-2701 (1988).
15. Ruiz-Ederra, J., García, M., Hicks, D., & Vecino, E. Comparative study of the three neurofilament subunits within pig and human retinal ganglion cells. *Mol. Vis.* **10**, 83-92 (2004).
16. Bringmann, A., Pannicke, T., *et al.* Müller cells in the healthy and diseased retina. *Prog. Retin. Eye Res.* **25**, 397-424 (2006).
17. Seo, J.M., Kim, S.J., *et al.* Biocompatibility of polyimide microelectrode array for retinal stimulation. *Mater. Sci. Eng. C.* **24**, 185-189 (2004).
18. Gerding, H., Benner, F.P., & Taneri, S. Experimental implantation of epiretinal retina implants (EPI-RET) with an IOL-type receiver unit. *J. Neural Eng.* **4**, S38-S49 (2007).
19. Majji, A.B., Humayun, M.S., *et al.* Long-term histological and electrophysiological results of an inactive epiretinal electrode array implantation in dogs. *Invest. Ophthalmol. Vis. Sci.* **40**, 2073-2081 (1999).
20. Walter, P., Szurman, P., *et al.* Successful long-term implantation of electrically inactive epiretinal microelectrode arrays in rabbits. *Retina.* **19**, 546-552 (1999).
21. Pardue, M.T., Stubbs, E.B., Jr., *et al.* Immunohistochemical studies of the retina following long-term implantation with subretinal microphotodiode arrays. *Exp. Eye Res.* **73**, 333-343 (2001).
22. Gekeler, F., Szurman, P., *et al.* Compound subretinal prostheses with extra-ocular parts designed for human trials: successful long-term implantation in pigs. *Graefes. Arch. Clin. Exp. Ophthalmol.* **245**, 230-241 (2007).
23. Montezuma, S.R., Loewenstein, J.I., Scholz, C., & Rizzo, J.F., III. Biocompatibility of materials implanted into the subretinal space of Yucatan minipigs. *Invest. Ophthalmol. Vis. Sci.* **47**, 3514-3522 (2006).
24. Montezuma, S.R., Loewenstein, J.I., Scholz, C., & Rizzo, J.F., III. Biocompatibility of materials implanted into the subretinal space of Yucatan minipigs. *Invest. Ophthalmol. Vis. Sci.* **47**, 3514-3522 (2006).
25. Ray, A., Colodetti, L., *et al.* Immunocytochemical analysis of retinal neurons under electrical stimulation. *Brain Res.* **1255**, 89-97 (2009).
26. Nakauchi, K., Fujikado, T., *et al.* Threshold suprachoroidal-transretinal stimulation current resulting in retinal damage in rabbits. *J. Neural. Eng.* **4**, S50-S57 (2007).
27. Shepherd, R.K., Murray, M.T., Houghton, M.E., & Clark, G.M. Scanning electron microscopy of chronically stimulated platinum intracochlear electrodes. *Biomaterials.* **6**, 237-242 (1985).
28. Villalobos Villa, J. *Safety of a Wide-Field Suprachoroidal Retinal Prosthesis*., Doctor of Philosophy thesis., The University of Melbourne., (2012).
29. Nayagam, D.A. X., Allen, P.J., *et al.* In: *A Pre-Clinical Model for Chronic Electrical Stimulation of the Retina via Suprachoroidal Electrodes, Association for Research in Vision and Ophthalmology Annual Meeting.*, **Vol. 5540/D1145**, Fort Lauderdale, Florida, USA, (2012).
30. Nayagam, D.A. X., Villalobos, J., *et al.* in *A Suprachoroidal Retinal Prosthesis is Safe in a Chronic Implantation Model, The Association for Research in Vision and Ophthalmology Annual Meeting.*, **Vol. 4928/A327**, Fort Lauderdale, Florida, USA, (2011).
31. Cicione, R., Shivdasani, M.N., *et al.* Visual cortex responses to suprachoroidal electrical stimulation of the retina: effects of electrode return configuration. *J. Neural Eng.* **9**, 036009 (2012).
32. Schuettler, M., Stiess, S., King, B.V., & Suaning, G.J. Fabrication of implantable microelectrode arrays by laser cutting of silicone rubber and platinum foil. *J. Neural Eng.* **2**, S121-S128 (2005).
33. Morimoto, T., Kamei, M., *et al.* Chronic implantation of newly developed suprachoroidal-transretinal stimulation prosthesis in dogs. *Invest. Ophthalmol. Vis. Sci.* **52**, 6785-6792 (2011).
34. Bron, A.J., Tripathi, R.C., & Tripathi, B.J. *Wolff's anatomy of the eye and orbit*,. Arnold, (2001).
35. Stein, J.J., Johnson, S.A., & Berson, D.M. Distribution and coverage of beta cells in the cat retina. *J. Comp. Neurol.* **372**, 597-617 (1996).
36. Dagnelie, G. Psychophysical evaluation for visual prosthesis. *Annu. Rev. Biomed Eng.* **10**, 339-368 (2008).